2004

Speciation of Organic Aerosols in the Tropical Mid-Pacific and their Relationship to Light Scattering

Crahan, Kathleen K.

Speciation of Organic Aerosols in the Tropical Mid-Pacific and Their Relationship to Light Scattering

KATHLEEN K. CRAHAN, DEAN A. HEGG, AND DAVID S. COVERT

Department of Atmospheric Sciences, University of Washington, Seattle, Washington

HAFLIDI JONSSON

CIRPAS, Marina, California

JEFFREY S. REID

Naval Research Laboratory, Monterey, California

DJAMAL KHELIF

University of California, Irvine, Irvine, California

BARBARA J. BROOKS

University of Leeds, Leeds, United Kingdom

(Manuscript received 23 July 2003, in final form 31 March 2004)

ABSTRACT

Although the importance of the aerosol contribution to the global radiative budget has been recognized, the forcings of aerosols in general, and specifically the role of the organic component in these forcings, still contain large uncertainties. In an attempt to better understand the relationship between the background forcings of aerosols and their chemical speciation, marine air samples were collected off the windward coast of Oahu, Hawaii, during the Rough Evaporation Duct project (RED) using filters mounted on both the Twin Otter aircraft and the *Floating Instrument Platform* (*FLIP*) research platform. Laboratory analysis revealed a total of 17 species, including 4 carboxylic acids and 2 carbohydrates that accounted for 74% ± 20% of the mass gain observed on the shipboard filters, suggesting a possible significant unresolved organic component. The results were correlated with in situ measurements of particle light scattering (σ_{sp}) at 550 nm and with aerosol hygroscopicities. Principal component analysis revealed a small but ubiquitous pollution component affecting the σ_{sp} and aerosol hygroscopicity of the remote marine air. The Princeton Organic-Electrolyte Model (POEM) was used to predict the growth factor of the aerosols based upon the chemical composition. This output, coupled with measured aerosol size distributions, was used to attempt to reproduce the observed σ_{sp}. It was found that while the POEM model was able to reproduce the expected trends when the organic component of the aerosol was varied, due to large uncertainties especially in the aerosol sizing measurements, the σ_{sp} predicted by the POEM model was consistently higher than observed.

1. Introduction

The global radiative budget is a balance sensitive to many factors. While the positive forcing of greenhouse gases is well established, aerosols also play an important role by their generally net negative forcing of the radiative budget due to their backscatter of incoming solar radiation. Although the direct forcing of several inorganic compounds, especially sulfates, has been well documented (Charlson et al. 1992), the radiative forcing budget of aerosols in general, and of organic aerosols in particular, still contain large uncertainties (Houghton et al. 2001, 392–393).

The amount of light scattering generated by an aerosol layer remains a difficult quantity to parameterize due to its dependence on a large number of interdependent variables including aerosol concentration, shape, size distribution, and chemical composition. While exploration of all of these relationships is necessary to understand the behavior of aerosols, this paper focuses on the phenomenological relationship of the chemical composition of aerosols, the ambient relative humidity, and the aero-

Corresponding author address: Kathleen Crahan, Department of Atmospheric Sciences, University of Washington, Box 351640, Seattle, WA 98195-1640.
E-mail: katie@atmos.washington.edu

sol scattering coefficient. The relationship defining the dependence of aerosol light scattering on relative humidity (RH) has been described by Katzen (1969) as [see also Gassó et al. (2000)]

$$\sigma_{sp} = k\left(1 - \frac{RH}{100}\right)^{-\gamma}, \quad (1)$$

where σ_{sp} is the particle scattering coefficient, RH is the ambient relative humidity, and k and γ are determined by fitting the equation to known data. In principle k is σ_{sp} (RH = 0) and γ alone defines the aerosol hygroscopicity (Gassó et al. 2000) with higher γ values associated with more hygroscopic aerosols (i.e., those whose light scattering is more strongly dependent on RH). Scattering measurements can be taken at two different relative humidities, eliminating the need to determine k in Eq. (1), and the γ value can be determined through fitting the curve to such in situ measurements.

The linkage between aerosol composition and hygroscopic growth is strong (Maßling et al. 2003) and, in principle, one can also determine the aerosol hygroscopicity from the chemical composition of ambient aerosols utilizing theoretical analysis. The current unsatisfactory state of solution theory for the complex chemical mixtures of organics and inorganics that constitute ambient aerosols renders a theoretical, first-principles approach difficult, but recent models have significantly improved the estimation of the complex chemical interactions of aerosols in response to changes in their environment.

The organic component within marine aerosols may be due to long-range transport of pollution or may be a result of the breakdown products of marine phytoplankton (Ellison et al. 1999). The effect of organics on the hygroscopic growth and deliquescence relative humidity (DRH) depends upon the solubility of the organics. In general, smaller chained organics and those with more carboxyl and alcohol functional groups are more soluble in water and in solution they lower the activity of water and thus the free energy of the system, producing a lower DRH and enhancing aerosol growth at lower relative humidities. However, a longer chained organic with fewer functional groups has the opposite effect, inhibiting deliquescence. Beyond the DRH the organics in solution constrain the influence of the solute effect such that an aerosol containing organics does not grow as much as one containing pure inorganics at the same RH below its critical radius (Ming and Russell 2002).

The surfactant properties of organics also play an important kinetic role in the growth of aerosols. The tendency of the organics to form a film on the surface of the aerosol (Ellison et al. 1999) inhibits the movement of water in and out of the aerosol solution, causing the response to lag with changes in relative humidity. Delays of 6–10 s have been observed for sulfuric acid droplets coated with lauric, stearic, and oleic acids to reach their equilibrium radius (Xiong et al. 1998) and of up to 30 s in cloud droplet formation observed within a cloud condensation nuclei (CCN) static diffusion chamber (Bigg 1986).

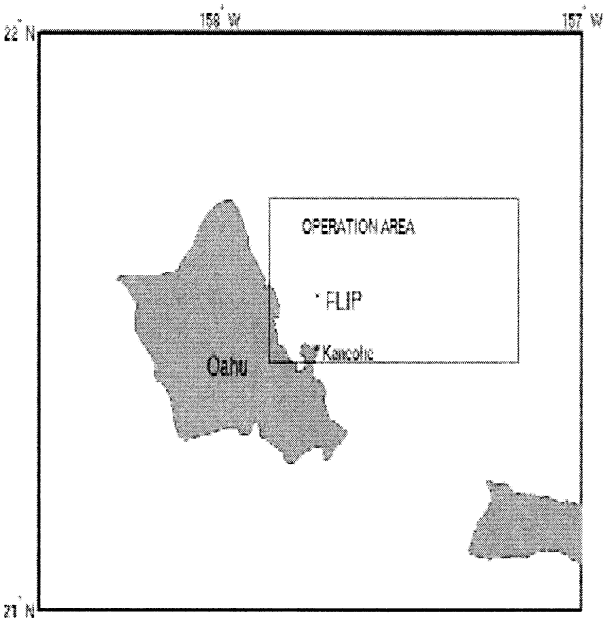

FIG. 1. Map of Oahu showing the operation area of the RED field campaign.

The venue of the Rough Evaporation Duct project (RED) off the eastern shore of Oahu, Hawaii, (conducted during August and September of 2001), was well suited to study the hygroscopicity and scattering of background marine aerosols. The presumably background nature and thus simplicity of the aerosol facilitates exploration of the linkage between chemical composition and hygroscopic and optical properties, and the incorporation of the organic species into current aerosol hygroscopic models. In this paper we will concentrate on the organic component of the aerosol, exploring possible sources as well as their effects on the particle light scattering and aerosol hygroscopicity. We will also attempt to reproduce these observations using a thermodynamical model, based upon the chemical composition of the aerosols, that predicts the growth factor of the aerosol.

2. Methodology

RED employed two aerosol sampling platforms, one aboard the Center for Interdisciplinary Remotely Piloted Aircraft Studies (CIRPAS) Twin Otter (TO) aircraft based out of Kaneohe Marine Corps Air Base on Oahu and a second upon the *Floating Instrument Platform* (*FLIP*) research vessel that was moored off the northeastern shore of Oahu (21.7°N, 157.8°W), as illustrated in Fig. 1.

The TO was equipped with an air intake probe with

an approximately 50% cutoff point of 8 μm, which was used to sample several intrinsic aerosol properties including the particle light scattering coefficient. The instruments employed included the University of Washington passive humidigraph (UWPH), which measured light scattering using two single wavelength (540 nm) nephelometers (Model 903, Radiance Research, Seattle, Washington) at two different RHs of nominally 44% and 86% (Gassó et al. 2000) and a TSI nephelometer (Model 3563, TSI, St. Paul, Minnesota), which measured scattering at three wavelengths (450, 550, and 700 nm) at a relative humidity of approximately 43%. The corrections for angular truncation and a non-Lambertian light source described by Anderson and Ogren (1998) were applied to the collected data, with additional corrections made for the larger angular truncation within the UWPH nephelometer compared to the TSI nephelometer and for a heater component inserted within the TSI nephelometer. The heater component also further limited the aerosol cutoff point within the nephelometer to approximately 4 μm.

The Passive Cavity Aerosol Spectrometer Probe 100x (PCASP) and Forward Scattering Spectrometer Probe 100 (FSSP; PMS/DMT Inc., Boulder, Colorado) were external optical probes aboard the TO used to measure aerosol size distributions, each utilizing 20 separate size bins. The PCASP measured accumulation mode aerosols with diameters ranging from 0.106 to 3.5 μm at an RH of approximately 35%, while the FSSP measured coarse mode aerosols with diameters between 1.5 and 44 μm at ambient RH. *FLIP* was equipped with a PCASP-100x and an FSSP-100, functioning at nominal RHs of 50% and ambient, relatively. While the PCASP instrument aboard *FLIP* was similar to that aboard the TO, *FLIP* was run at a higher gain, with a maximum diameter of 25 μm. Both platforms utilized similar aerosol particle sizers (APS Model 3020, TSI) which measured aerosols of mean diameters between 0.36 to 14.5 μm. The FSSPs and PCASPs were calibrated using glass and latex beads of known size and refractive index as described by Liu et al. (1992).

Thirty aerosol filter samples were collected using the TO aircraft both within the marine boundary layer and extending up to 2100 m above sea surface over the course of 12 days using a pump that drew air at a rate of 100 lpm and with variable collection times of at least 16 minutes. A Micro Orifice Impactor (MOI) with its impactor stages removed was mounted on the wing of the TO and was used as a standard aerosol filter sampler (a final 90-mm Zeflour filter collected all sizes) with an upper 50% aerosol cutoff of approximately 3.5 μm, as described by Gao et al. (2003). The MOI was designed to be isokinetic at a flow rate of 100 L min^{-1} and contained eight cassettes with the flow to each cassette electronically controlled from within the TO. After collection, the filters were stored at a nominal 5°C to minimize volatilization. MOI blank filters, stored under the same conditions as the exposed filters, were used for subtraction of any background aerosol loading accumulated during the handling of the filters.

In conjunction with the TO, *FLIP* employed a filter sampler for surface level aerosol measurements. The intake was a 1-m-long 316 stainless steel pipe aligned with the mean wind with a 1.7-cm internal diameter and approximate cutoff point of 10 μm, dependent upon wind speed. A total of 20 samples were collected between 1100 and 1700 local time, at a rate of one per day, using Zeflour 90-mm filters employing a pump that drew 100 L min^{-1} of air through the filters. The exposed filters were stored in conditions similar to the exposed TO filters. Blanks were also employed.

Gravimetric analysis was performed on the *FLIP* filters. The filters were weighed in a clean box kept at approximately 20°C $\pm$ 3°C and 43% $\pm$ 2% relative humidity. The masses of the filters were obtained before and after exposure and the masses of the aerosol loading on the filters were deduced with an accuracy of $\pm$3%.

The filters were extracted using 10 mL aliquots of high-performance liquid chromatography (HPLC)-grade water and underwent vigorous agitation to remove all aerosol species. It can be assumed that the extraction process removed all soluble and moderately soluble species including a number of organic species, and that the particulate oxide components were suspended in solution due to the vigorous agitation. Subsequently, the solution was divided into four separate aliquots for chemical analysis, as detailed by Gao et al. (2003). Inductively Coupled Plasma Atomic Emission Spectrometry (ICP-AES, model ASU 955, Jarrell Ash, Grand Junction, Colorado) was able to identify seven metals, Ca, Fe, K, Mg, Na, Si, and Al, within an accuracy ranging from 3% to 10%. Ion chromatography (model DX-500, Dionex, Sunnyvale, California) in the conductivity mode was able to identify sulfate, nitrate, phosphate, chloride, glutarate, succinate, and oxalate with an accuracy better than 15% for the inorganic species and 29% for the dicarboxylic acids. Examination using electrospray ionization–ion trap mass spectrometry (model Esquire-LC, Bruker/Hewlett-Packard, Billerica, Massachusetts) coupled with ion chromatography in the pulsed amperometric detector (PAD) mode, identified glucose and levoglucosan with an accuracy better than 14%.

3. Results

a. Experimental

The meteorological conditions measured during the campaign suggested that the air sampled by the TO and *FLIP* was representative of a well-mixed marine boundary layer, as expected based on previous campaigns (Albrecht et al. 1995). Figures 2 and 3 show little variation with altitude of wind speed, wind direction, equivalent potential temperature, and dewpoint below 1000 m MSL, suggesting that air masses at different altitudes

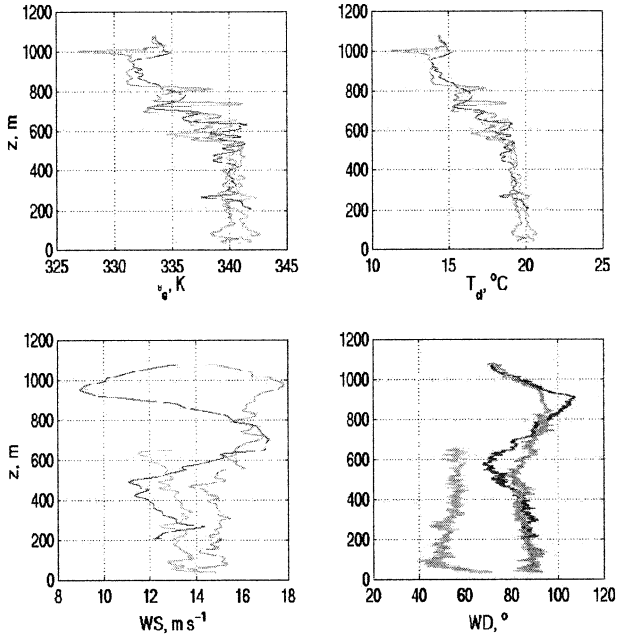

FIG. 2. Profiles of equivalent potential temperature (θ_e), dewpoint temperature (T_d), wind speed (WS), and wind direction (WD) for 30 Aug 2001, indicating a well-mixed boundary layer. (Data are obtained from the Twin Otter soundings.)

had the same source. To strengthen this assumption, the level of correlation was explored between the measurements made on *FLIP* and the lowest-level passes of the TO near *FLIP* (below 100 m MSL). The data collected from the PCASP and FSSP aboard the two platforms were compared and the results correlating the aerosol

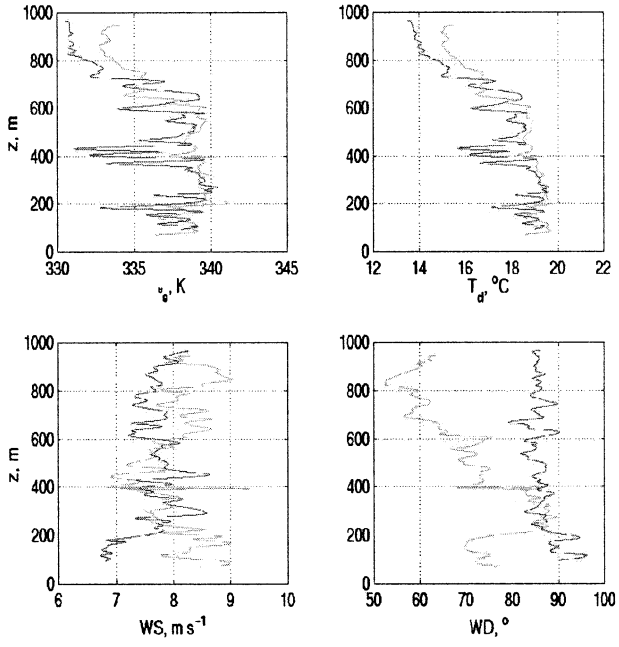

FIG. 3. As in Fig. 2 except for 4 Sep 2001.

TABLE 1. Examining the level of correlation between the TO and *FLIP* based upon aerosol number concentration (particles per cubic centimeter) measured by the FSSP and PCASP on the two platforms. The observed number concentrations and results of a simple Pearson correlation include the dates compared and the correlation coefficient.

	PCASP					
	Fine mode		Coarse mode		FSSP	
Date	*FLIP*	TO	*FLIP*	TO	*FLIP*	TO
30 Aug 2001	141.7	135.8	4.08	1.13	2.17	0.44
4 Sep 2001	109.2	97.2	0.95	0.35	0.69	0.18
10 Sep 2001	223.3	195.1	3.77	1.28	2.17	0.39
14 Sep 2001	116.9	101.6	1.60	0.39	1.01	0.18
R^2	0.968		0.989		0.975	

number concentration for the PCASP submicron and supermicron mode, as well as for the total FSSP number concentration are reported in Table 1. Although only four cases were available for comparison when the PCASP and FSSP were functioning on both platforms, the coefficients of correlation between the surface and the aircraft measurements were very high ($R^2 = 0.96$) as would be expected in the case of a well-mixed layer. Additionally, the APSs aboard the two platforms showed a high level of correlation, as illustrated in Fig. 4. The number concentration measurements show the PCASP fine modes correspond well at 15 and 100 m MSL, but there is a noticeable drop in coarse mode concentrations as measured by the TO below 100 m, although the time trends are similar between platforms. This trend is reflected in the aerosol size distributions measured from the two platforms. The surface area aero-

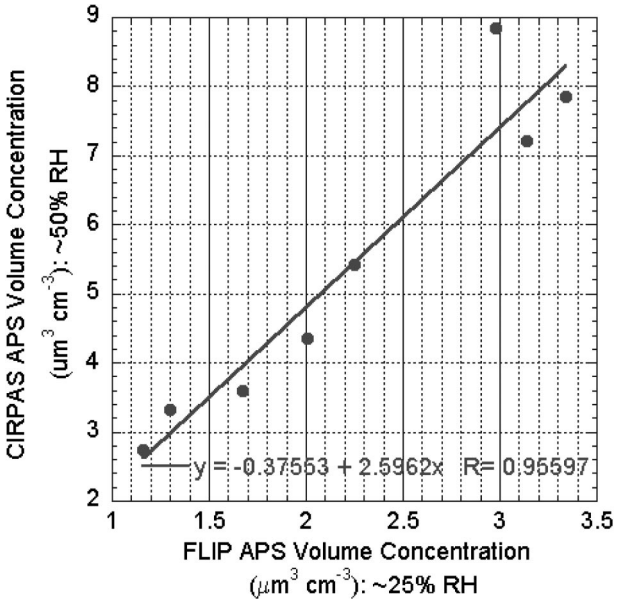

FIG. 4. A comparison of the size distributions measured using the APS aboard the two platforms. Throughout the campaign, there was a high degree of correlation ($R^2 > 0.95$) and a slope greater than one due to differences in the RHs of the two instruments.

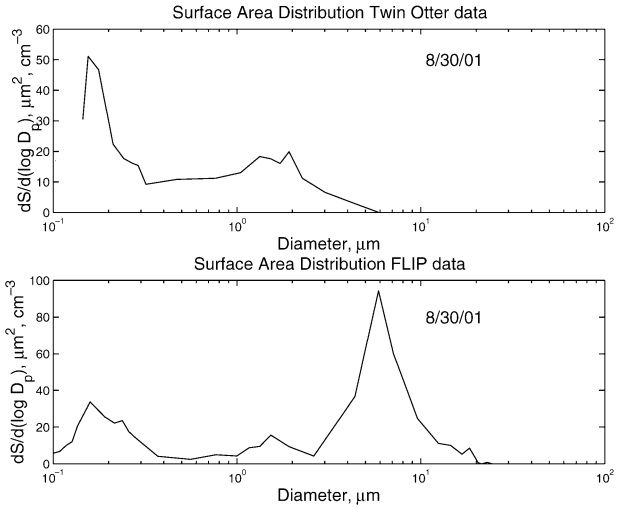

FIG. 5. A comparison of the size distribution measured using the PCASP and FSSP aboard the two platforms during sample FLIP 04 on 30 Aug 2001, a marine-1 case. The TO data are from the lowest-level overpasses of *FLIP*. While the accumulation modes measured are comparable, there is a slight decrease with increasing altitude in the coarse mode surface area concentration and mean diameter. The RHs of the four instruments were 33% (TO-PCASP), 69% (TO-FSSP), 50% (*FLIP*-PCASP), and 75% (*FLIP*-FSSP).

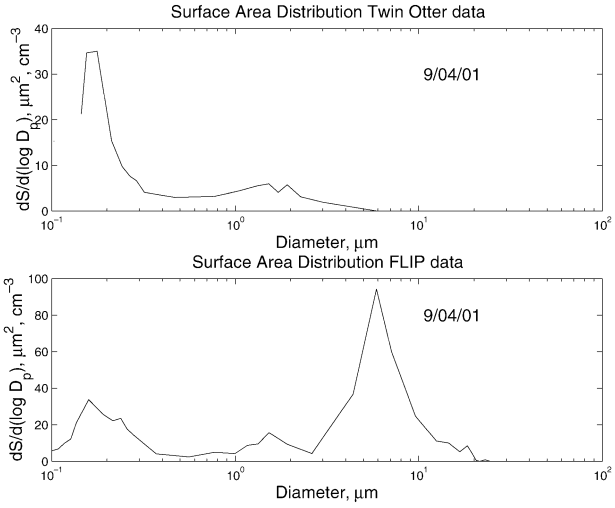

FIG. 6. A comparison of the size distribution measured using the PCASP and FSSP aboard the two platforms during 4 Sep 2001, again demonstrating a slight decrease with increasing altitude in the coarse mode number concentration and mean diameter. The RHs of the four instruments were 33% (TO-PCASP), 70% (TO-FSSP), 50% (*FLIP*-PCASP), and 75% (*FLIP*-FSSP).

sol size distributions for 30 August and 4 September taken from *FLIP* and the lowest-level *FLIP* overpasses of the TO can be seen in the size distributions measured from the TO and *FLIP* shown in Figs. 5 and 6. It can be seen that, while the submicron aerosol distribution from the two platforms are similar, there is a decrease in the total aerosol number and mean diameter in the supermicron aerosol size distribution as measured from the TO. Some of this discrepancy in the sea salt measured size distributions may be due to variable hygroscopicity and the presence of organics (Reid et al. 2001). The difference in gains used in the FSSPs aboard the two platforms also likely impacted the measured size distributions. Reid et al. (2003, 2001) found that the FSSP consistently oversized dust particles. Current work by Reid et al. (2004, unpublished manuscript) shows that the FSSP on *FLIP* oversized the volume mean diameter by as much as 60%. This anomalous oversizing may be due to the higher gains used on the *FLIP* FSSP where the inflexion in the Mie scattering in the 3–8-μm range caused increased probability of a particle being oversized.

The strong level of correlation between the instruments on the two platforms coupled with the soundings data further indicate that a well-mixed marine boundary layer was present during the campaign. This implies that the chemistry between the two levels can be assumed to be similar as well. To further investigate this, the chemical speciation observed on TO filters collected at the lowest-level *FLIP* passes on three occasions were compared to corresponding *FLIP* filter chemical speciation. While the total chemical mass resolved on the TO was less than on *FLIP*, the resolved inorganic and organic species were compared and the level of correlation between the fifteen species identified on the two filters collected on the same day was high. The results are shown in Table 2.

Due to the lack of scattering measurements on board *FLIP*, the γ values and corrected dry 550-nm σ_{sp} measured aboard the TO were collated with *FLIP* filters whenever possible, using only the data collected during TO passes under 100 m MSL. Additional conditional sampling was performed to ensure that only cases in which γ was essentially constant from pass to pass were utilized. This was done because the filter sampling intervals subsumed many TO passes and variations between γ and composition could add noise to the data. The 550-nm σ_{sp} was correlated with nine *FLIP* filter analyses, and γ values were determined for seven cases. The γ values were calculated as described in Eq. (1) using the UWPH nephelometers at a wet RH of 86% $\pm$ 5% (mean and standard deviation) and a dry RH of 44% $\pm$ 10% and a wavelength of 540 nm. (The 550 nm dry σ_{sp} and γ values associated with the filters are reported in Figs. 7 and 8.)

Backward trajectory analysis with Hybrid Single-Par-

TABLE 2. Examining the level of correlation between the TO and *FLIP* chemical concentrations: results of a simple Pearson correlation of the 15 chemically resolved species from the TO and *FLIP* filters including R^2, where R is the correlation constant.

Date	Filters	R^2
28 Aug	TO10, FP02	0.847
30 Aug	TO19, FP04	0.801
5 Sep	TO55, FP11	0.983

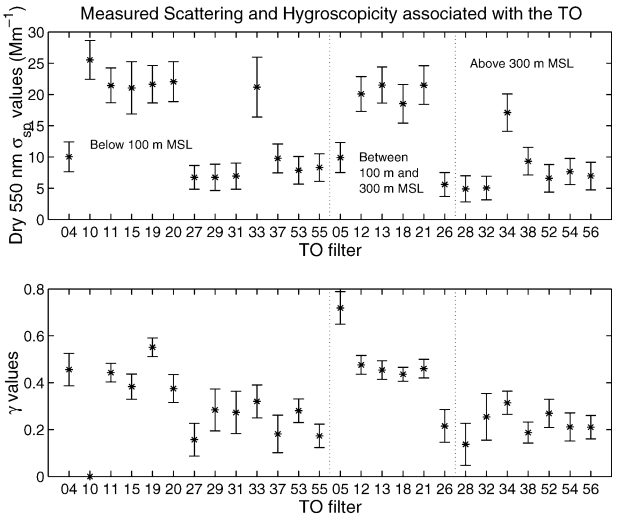

FIG. 7. A summary of the (top) 550-nm dry σ_{sp} scatter and (bottom) γ values and the measurement standard deviation associated with the Twin Otter filters calculated from measurements of the UWPH and TSI nephelometer aboard the TO. Reported values of zero correspond with filters for which no data are available.

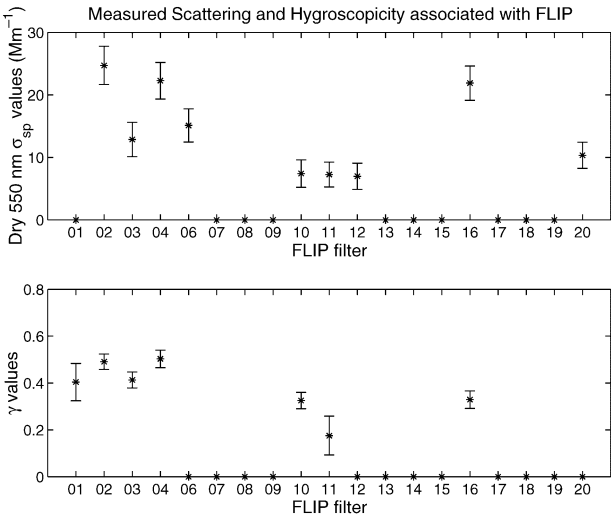

FIG. 8. As in Fig. 7 except for the *FLIP* filters during several passes over the *FLIP*. Reported value of zero corresponds with the filter for which no data are available.

ticle Lagrangian Integrated Trajectory Model (HYSPLIT4) (Draxler 1997) with initialization at 200 m above the FLIP coordinates showed that the air masses observed during the campaign passed through two different geographic locations 144 h prior to arriving in the study area. Although the primary air mass was marine air arriving from east of Oahu (23°–48°N, 128°–152°W), late August also saw several instances of coastal air, air masses that passed southeast of the sampling platforms skimming along the edges of several of the islands south of Oahu before arriving at the aerosol sampling platforms of RED (23°–25°N, 125°–137°W). Additionally, the marine air can be divided into two distinct categories. During the beginning of the campaign the trade winds over Oahu were strong and the air masses sampled were most representative of the marine air expected throughout the campaign. After 1 September 2001 there was a drop in the average local wind speeds. This reduction in strength in the trade winds was also marked by a larger degree of variability in wind direction, with the winds occasionally becoming southerlies or southeasterlies. The marine air masses associated with the strong trade winds are henceforth referred to as marine-1 and the air masses seen in the latter portion of the campaign are termed marine-2. For at least one date for each case, the HYSPLIT4 was also run using an initiation altitude of 100 and 500 m, producing only minor deviations of a few degrees in the back trajectories 144 h upwind, as expected in a well-mixed marine boundary layer situation.

Summaries of the chemical speciation results are plotted in Figs. 9 and 10. While sodium was not found on some of the TO filters due to the high limit of detection associated with the ICP (approximately 0.3 μg m^{-3}, dependent on sample time), in cases containing sodium, there is evidence of chloride depletion, indicative of acidic sulfate or nitrate possibly of anthropogenic origin, with the TO filter depletion varying between 0% and 52% loss and the *FLIP* filter depletion ranging from 14% to 48%. While encompassing a large range, it is consistent with previous campaigns where the chloride depletion of marine air ranged between 5% and 30% off the Netherlands coast (Ten Harkel 1997) and from 0% to 100% in the remote southern Pacific Ocean

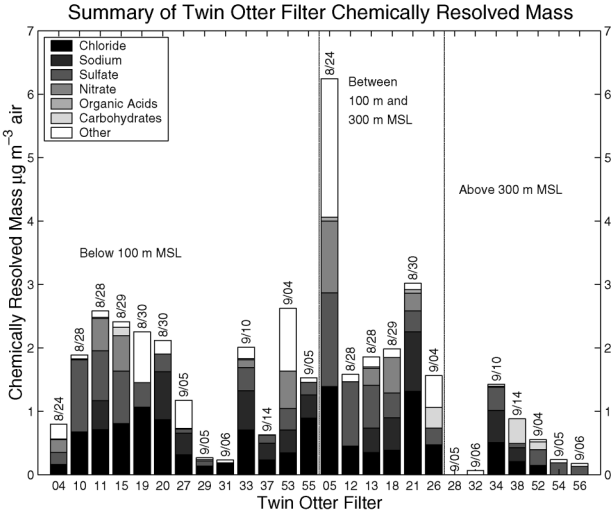

FIG. 9. A summary of the chemical mass resolved from the filters collected aboard the Twin Otter and their corresponding dates of collection. The first 13 filters were collected below 100 m MSL, the next 5 were between 100 and 300 m MSL, and the final 8 were collected above 300 m MSL. Samples collected 24 and 29 Aug through 1 Sep correspond to marine-1 air masses, samples collected 27 and 28 Aug are coastal air masses, and samples collected 2 Sep and later were termed marine-2 air masses.

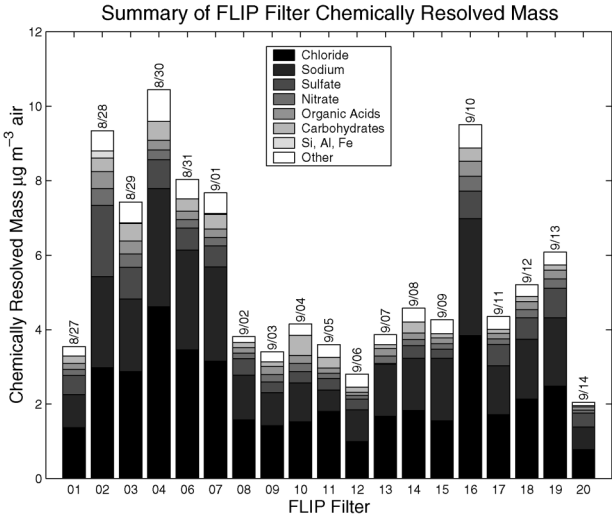

FIG. 10. A summary of the chemical mass resolved from the filters collected aboard *FLIP* (approximately 15 m MSL) and their corresponding dates of collection. Samples collected 24 and 29 Aug through 1 Sep correspond to marine-1 air masses, samples collected 27 and 28 Aug are coastal air masses, and samples collected 2 Sep and later were termed marine-2 air masses.

(McInnes et al. 1994). That the observed air masses are not always representative of pure marine aerosol is further supported by the presence of iron, aluminium, and silicon found on three *FLIP* filters, metals in their oxide forms that are common in volcanic and soil dust. Although calcium and magnesium are also common crustal metals, they are found in significant concentrations in seawater salts and no assumptions were made concerning the origins of those metals. The results are consistent with a previous campaign conducted on Oahu in 2000, which found evidence of long-range transport based upon nephelometer data and backtrajectory analyses (Clarke and Kapustin 2003).

Several dicarboxylic acids and carbohydrates were observed in the filter samples. Although the presence of glucose and levoglucosan, common biomass burning tracers, may initially seem confusing, analysis of sea surface waters for organics revealed a significant carbohydrate concentration, including glucose (Aluwihare et al. 1997). Additionally, recent works (Simoneit et al. 1999; Fraser and Lakshmanan 2000) show that levoglucosan is emitted at high concentrations in biomass burning and, as it is stable for up to 10 days, it may be used as a long-range tracer for biomass burning (a source of relatively hygrophobic aerosols). Satellite photos [Moderate-Resolution Imaging Spectrometer (MODIS) 14 *Terra*, collection 04] have revealed large burning areas on both the Big Island of Hawaii and in several spots on the west coast of the United States during the field campaign.

Analysis of the TO filters based on the airmass source revealed that the decrease in daily averaged wind speed is reflected in the stratified γ values associated with distinct air masses. Isolating the marine-1 air masses where the wind speeds averaged 9 ± 1 m s^{-1}, the average γ value is 0.48 ± 0.12, while the marine-2 air masses saw winds speeds only at 6.3 ± 0.7 m s^{-1} and the γ values dropped to 0.23 ± 0.06. The γ values for the coastal air averaged 0.45 ± 0.02. The drop in γ values during the latter portion of the campaign may be due to an increase in the anthropogenic component of the air, which is reflected in the nss sulfate mass concentration relative to the total resolved chemical mass. The marine-1 air contained only small portions of nss sulfate, contributing $8\% \pm 9\%$ to the total resolved mass, while the coastal air contained $37\% \pm 15\%$ and the relative amount in the marine-2 air was highly variable, at $17\% \pm 27\%$. The mean and standard deviation of the dry 550-nm σ_{sp} for the marine-1 air was 17.8 ± 5.4 Mm^{-1}. There was a slight increase in the σ_{sp} values during the coastal air incidences, averaging at 22.1 ± 2.3 Mm^{-1}, while the latter portion of the campaign saw a sharp decrease in σ_{sp}, with an average of 8.7 ± 4.5 Mm^{-1}.

Mass closure was performed on the *FLIP* filters by comparing the results of the gravimetric analysis to the resolved chemical concentrations. As discussed above, assuming that iron, silicon, and aluminium were captured in their oxide forms (Al_2O_3, Fe_2O_3, SiO_2) and disregarding the one case where over 100% of the gravimetric mass was resolved, on average only $74\% \pm 20\%$ of the gravimetric mass was resolved into its chemical components. A variety of explanations can be offered to explain this mass deficit of the chemically resolved components, including an underrepresentation of the organic fraction of the aerosol due to the difficulty of resolving low-solubility chemical components with the techniques utilized. In order to determine the total organic fraction in the aerosols observed, estimates were made of the nonorganic unresolved aerosol mass. To set the upper bound for the organic fraction, the possibility of unresolved heavy metals was first examined. It is unlikely that a significant portion of the gravimetric mass not accounted for by the chemical analysis could be due to heavy-metal enrichment of the marine brine, such as copper, cadmium, or manganese. Oppo et al. (1999) have found them present at levels only up to 2.1 ng m^{-3}. Ammonium, a significant contributor to marine aerosol mass, can be assumed to be present at a mass between 30 and 90 ng m^{-3} of air (Quinn et al. 1993; Adams and Seinfeld 1999). Taking these species into account an average of 29%–30% of the surface aerosol, including the average of 5% of the chemically resolved organics, could be attributable to organics. This number is compatible with previous measurements and can be used as an upper limit. To set a lower bound for the organic mass fraction in the aerosols, one can assume that the sulfate in the marine atmosphere was completely neutralized by ammonium rather than the more likely scenario that a significant portion of the sulfate aerosol takes the form of ammonium bisulfate. This assumption

TABLE 3. Chemical composition of aerosol sampled on board *FLIP*: results of principal component analysis with varimax rotation including the component loading and the percent variance explained by each component. The four components explained only 84% of the variance, and the remaining eigenvectors were eliminated due to low computational stability. The σ_{sp} values at the bottom of the table were the loadings on the four components when the PCA was redone to include the σ_{sp} associated with each filter. The changes of the chemical loadings associated with the new PCA were small.

Component	1 (33%)	2 (27%)	3 (13%)	4 (11%)
Calcium	0.897	0.120	−0.124	−0.053
Iron	0.129	0.954	0.002	0.194
Potassium	0.338	0.099	−0.053	0.330
Magnesium	0.911	0.061	0.136	0.329
Sodium	0.911	0.114	0.222	0.135
Silicon	0.084	0.966	0.105	0.032
Aluminum	0.247	0.912	−0.010	−0.214
Chloride	0.923	0.078	0.212	0.224
Nitrate	0.615	0.551	0.301	0.238
Glutarate	0.163	0.178	0.877	0.099
Succinate	0.174	0.160	0.302	0.852
Malonate	−0.095	0.130	0.841	−0.112
SS Sulfate	0.867	0.190	0.229	0.234
NSS Sulfate	−0.096	0.941	0.153	0.244
Oxalate	0.258	0.683	0.614	0.223
Phosphate	0.164	0.173	−0.450	0.738
Levoglucosan	0.824	0.093	−0.129	−0.126
Glucose	0.778	0.174	−0.331	0.184
σ_{sp}	0.51	0.44	0.59	0.42

yields aerosol ammonium concentrations as high as 720 ng m^{-3}. Additionally, water mass may account for some of the gravimetrically resolved mass. At an RH of 43%, Ming and Russell (2001) predict a diameter aerosol growth factor of approximately 1.1. Assuming a dry aerosol density of 1.9 g cm^{-3} and a volume-weighted average hydrated aerosol density of 1.7 g cm^{-3}, 18% of the gravimetrically resolved mass may be due to water on the aerosol. This, combined with the higher ammonium concentration calculated above, gives an average lower limit of total organics within the aerosol of 10%.

Principal component analysis (PCA) with varimax rotation was designed to look at joint variation between factors and group together those that have high covariance. The component loading within a factor indicates the level of covariance of the variable with the component and loadings of opposite signs indicate negative covariance. Varimax rotation relaxes the orthogonality of the eigenvectors in order to maximize component loadings. PCA was performed on the *FLIP* data and to eliminate components with low computational stabilities, factors with eigenvalues less than one were not reported. The variables were resolved into four components as shown in Table 3, and the level of variance within the dataset explained by each factor is reported at the top of the table. The first component shows an obvious marine forcing with strong loadings of sodium and chloride, as well as calcium and magnesium, which are found in salt form in ocean water. Glucose and levoglucosan are also strongly loaded on this component. This is suggestive of either a direct marine source for glucose, or that this component contains traces of biomass burning contaminants originating from either the west coast of North America or Hawaii.

The second component suggests an air mass strongly influenced by land with strong loadings of silicon, iron, and aluminum, typical of soil dust. Nitrate and non–sea salt (NSS) sulfate were also present, demonstrating anthropogenic pollutants to be well mixed with the dust in the second component. The strong oxalate loading in this component is not surprising, considering it is found in anthropogenic pollutants. Based upon this, we will consider this to be a pollution component.

The third and fourth components contain the remaining dicarboxylic acids as well as a significant oxalate loading. Their separation from the pollution and marine component may be due to their production through the photooxidation of either anthropogenic pollutants or marine fatty acids during aerosol transport. However, the separation of succinic acid from glutaric acid, oxalic acid, and malonic acid is more difficult to explain. Kawamura and Sakaguchi (1999) observed an increase in the C2/C4 and C3/C4 dicarboxylic acid ratio at lower latitudes in the northern Pacific. Possible explanations included oxalic and malonic acid being more abundantly produced in lower latitudes or the relatively high reactivity of succinic acid. It is also possible that the higher solubility of the C3 and C5 diacids as well as the relatively high acidity of the C2 diacid in comparison to succinic acid result in a stronger partitioning into the condensed phase, as suggested by Gao et al. (2001). These differences in formation rates, breakdown rates, and partitioning may be sufficient to explain the separate loadings.

The 550-nm σ_{sp} was correlated with nine *FLIP* filter analyses. PCA was performed on the filters for these days to determine the eigenvectors associated with the 550-nm σ_{sp} from the previous PCA in Table 3. The chemical loadings on the components remained essentially unchanged. There were significant σ_{sp} loadings on all four components: 0.512, 0.436, 0.590, and 0.419 for the first, second, third, and fourth components, respectively, suggesting the chemical components of all four eigenvectors played a significant role in influencing the σ_{sp}. The lack of a significant number of γ values correlated with the *FLIP* filters precluded their inclusion in the PCA.

To further explore the relationships between σ_{sp}, hygroscopicity, and chemical concentrations, multiple linear regression was performed on the chemical analysis results. Due to the strong NSS sulfate loading on the pollution component in the PCA and the lack of evidence of methane sulfonate (a tracer for phytoplankton activity that breaks down into sulfate) in the IC chemical analysis, it was assumed that the majority of the NSS sulfate had anthropogenic origins. The level of correlation between NSS sulfate and chloride was only 0.074, further stressing their independence. Multiple regression

TABLE 4. Results of the multiple regression analysis using chemical tracers to predict the sea salt and pollution contribution to σ_{sp}. The percent contribution is calculated by performing a regression analysis using the tracers and inserting the average concentrations of the markers into the resulting equation, dividing the resultant by the averaged σ_{sp}, and normalizing the end product. The contribution of the constant likely contains the contribution to the 550-nm particle scatter of the dicarboxylic acids.

Tracers	R^2	Contribution		
		Marine	Pollution	Constant
Na^{1+}, NSS SO_4^{2-}	0.847	80%	9%	11%
Cl^{1-}, NSS SO_4^{2-}	0.830	75%	10%	15%
Mg^{2+}, NSS SO_4^{2-}	0.771	61%	11%	28%
Avg		72%	10%	18%
Std dev		10%	1%	9%

analysis of the 550-nm σ_{sp} using chloride as a tracer for the marine component and NSS sulfate as a pollution airmass tracer yielded

$$\sigma_{sp} = 4.269[Cl^{1-}] + 7.411[\text{NSS } SO_4^{2-}] + 1.837 \quad (2)$$

with an adjusted R^2 value of 0.83. The coefficients are consistent with previously determined mass scattering coefficients of NSS sulfate and chloride (Penner et al. 1998; McGovern et al. 1999). The average concentrations of chloride and NSS sulfate observed on the *FLIP* filters throughout the campaign were inserted into Eq. (2) and the resultant was divided by the averaged dry σ_{sp} to determine the time-averaged contribution of each of the components to σ_{sp} as determined by these tracers. The normalized results yielded estimates that 75% of σ_{sp} is attributable to sea salt and 10% to the pollution, while the constant or residual explained 15% of the 550 nm σ_{sp}. The standard errors associated with the coefficients associated with chloride, NSS sulfate, and the constant were found to be, respectively, 0.772, 2.42, and 2.238. Using these and the average error resulting from laboratory analyses of the chloride and NSS sulfate concentrations within the aerosols (0.12 and 0.10, respectively), an error analysis using the propagation of error through a Taylor expansion of Eq. (2) was performed. The results yielded a 15% uncertainty in the contribution of chloride to σ_{sp}, a 6.5% uncertainty in the sulfate scattering component, and a 15% uncertainty in the constant contribution to σ_{sp}, demonstrating the robustness of this analysis.

The magnitude of the constant's contribution to σ_{sp} suggests that a significant amount of the σ_{sp} might be ascribable to the dicarboxylic acids, the third and fourth components from the PCA. However, the large uncertainty in the constant (over 100%) renders this speculative. Regression analysis was performed again to further explore this using chloride, NSS sulfate, and malonate as tracers. The coefficients determined from the analysis for malonate, NSS sulfate, chloride, and the constant were 204.653, 5.957, 4.155, and 0.279, respectively. The normalized percent contribution results show the contribution of the constant to σ_{sp} to be minimized to 2%, while the dicarboxylic acids contributed 18% to the σ_{sp}. To further test the robustness of the component contributions, the regression analysis was performed using other tracers for the sea salt component. The results are summarized in Tables 4 and 5. These results do suggest a small but real scattering contribution from the dicarboxylic acids.

To ensure that the high pollution contribution to the clean marine air was not due to island recirculations contaminating marine air, the regression analysis was redone subtracting the cases containing iron, silicon, and aluminium, likely dust contaminants from the island. This resulted in a reduction of the NSS sulfate average concentration from 0.171 to 0.099 $\mu g\ m^{-3}$, while the tracers used for sea salt decreased by less than 8% and σ_{sp} was reduced by only 9%. However, linear regression analysis using the tracers of nss sulfate and chloride demonstrated that pollution was still responsible for 22% of the scattering, with sea salt contributing 66% of the scattering, and the constant accounting for 12% of the scattering. Adding and subtracting the standard error associated with the linear regression coefficients varied the pollution contribution from 19% to 28%, and using magnesium and sodium for sea salt tracers changed the pollution contribution from 21% to 27%. This reiterates the importance of the contribution of pollution to σ_{sp} in what has been considered clean marine air.

Similar multiple regression analysis performed on the γ values associated with the *FLIP* filters failed to yield significant results, due in part to the small number of cases and also to the fact that while σ_{sp} is strongly correlated to the mass concentrations, hygroscopicity is de-

TABLE 5. Results of the multiple regression analysis using chemical tracers to predict the sea salt, dicarboxylic acid, and pollution contribution to σ_{sp}. The contribution of the constant to the 550-nm particle scatter is significantly decreased while the dicarboxylic acids contributed to 15% on average of the scattering.

Tracers	R^2	Contribution			
		Marine	Pollution	Dicarboxylic acid	Constant
Na^{1+}, NSS SO_4^{2-}, malonate	0.940	76%	7%	16%	1%
Cl^{1-}, NSS SO_4^{2-}, malonate	0.935	72%	8%	18%	2%
Mg^{2+}, NSS SO_4^{2-}, malonate	0.861	58%	9%	18%	15%
Avg		69%	8%	17%	6%
Std dev		9%	1%	1%	8%

TABLE 6. Twin Otter chemical composition principal component analysis results with varimax rotation including the component loading and the variance explained by each component.

Component	1 (27%)	2 (23%)	3 (14%)	4 (9%)
σ_{sp}	0.763	0.549	0.175	0.121
γ	0.786	0.252	0.369	0.092
Chloride	0.388	0.823	−0.214	−0.159
Nitrate	0.574	0.166	0.157	−0.654
Succinate	−0.231	0.672	0.134	−0.014
Oxalate	0.285	0.623	0.352	0.321
Phosphate	0.580	0.050	0.573	0.018
Calcium	−0.130	−0.016	0.143	−0.856
Potassium	0.006	−0.026	−0.762	0.087
Magnesium	0.016	0.436	0.056	0.240
Sodium	0.030	0.904	0.204	−0.151
NSS Sulfate	0.927	−0.048	0.017	0.004
SS Sulfate	0.398	0.824	−0.218	−0.163
Levoglucosan	0.568	−0.086	−0.507	−0.258
Glucose	−0.158	−0.082	−0.715	0.162

pendent on a number of nonlinear interactions between the chemical components as well as the size distributions, making a linear fit more problematic.

Performing similar analyses on the TO filter results, again filtering out all factors with an eigenvalue less than one, the PCA once more revealed four factors, shown in Table 6. The first factor, heavily loaded with NSS sulfate and nitrate, represents the pollution component of the air mass. The marine air component revealed in the analysis is heavily loaded with sodium, chloride, and sea salt (SS) sulfate. Additionally, succinate and oxalate have become heavily associated with the marine component. This can be rationalized by assuming that the marine chemical component sampled at the higher altitudes is more representative of aged marine aerosols into which the breakdown products of marine fatty acids are better mixed. This is in agreement with Kawamura and Sakaguchi (1999) who speculated on the production of small diacids during long-range atmospheric transport of organic marine aerosols. Interestingly, levoglucosan is most strongly associated with the land-influenced pollution factor, implying that the pollution component represents the long-range transport of anthropogenically produced aerosols from North America. The lack of data points for the C3 and C5 dicarboxylic acids, as well as for silicon, aluminum, and iron precluded their inclusion in the PCA.

The third and fourth components, containing potassium, phosphate, calcium, nitrate, glucose, and levoglucosan may be due to the small influence of island air during the days of weak trade winds when the wind shifted to the south or southeast. The glucose and levoglucosan may be associated with a fire from the Big Island of Hawaii. Phosphate is positively loaded on the third component, while levoglucosan and glucose are negatively loaded. While the significance of this is not clear, it may be due to the positive correlation of phosphate to hygroscopicity, which is lightly loaded on the third component, while the carbohydrates would have the effect of suppressing the γ values.

Examining the γ values and 550-nm σ_{sp} loadings, γ and σ_{sp} both seem to be most strongly associated with the pollution component. The σ_{sp} also has a high loading on the sea salt component but this is surprisingly not shared by γ. Only weak associations with the remaining two factors are found for both σ_{sp} and γ. Performing linear regressions on σ_{sp} using NSS sulfate as a tracer for the primary pollution component captured by the TO filters, and sodium, chloride, or sea salt sulfate as tracer of the marine component, the percent contributions of these two components were derived as described previously. The adjusted multiple r^2 values were lower than found in the *FLIP* analysis, ranging from 0.739 to 0.765. The marine contribution to σ_{sp} was determined to be 45% ± 15%, and the pollution contribution was 21% ± 7%. The constant carried a heavy weighting of 33% ± 8%. The decrease in the relative contribution of sea salt to the TO σ_{sp} values compared to the *FLIP* regression can be explained by the greater sea salt concentration found at lower altitudes near the surface of the ocean.

Again, multiple regression performed on the γ values yielded lower adjusted multiple r^2 values, ranging between 0.561 and 0.653, but the higher number of cases suggested the results were significant. Using the same tracers as in the analysis of the TO σ_{sp}, the marine contribution to γ was 22% ± 14% and the pollution contribution was 18% ± 5%, while a heavily loaded constant explained 59% ± 9%.

While heavy contribution of the constant to both σ_{sp} and γ in the TO results may be due to the contributions of components three and four found in the PCA results, it could also be due to unresolved chemical components, such as long-chained organics within the aerosols, which could have the effect of significantly depressing the σ_{sp} and hygroscopicity of the aerosols. Better resolution of the mildly water soluble component of the aerosols is necessary to support this.

b. Model

The Princeton Organic-Electrolyte Model (POEM) code was originally created by Ming and Russell (2002) to address a gap in understanding of the thermodynamic behavior of organic aerosols. The model calculates the phase equilibrium of an aerosol of specified chemical content at a given ambient relative humidity by minimizing the Gibbs free energy of the system. The nonlinear contributions of inorganic components to Gibbs free energy have been described by Clegg et al. (1992). Nonlinearities of the interactions of the organics with each other as well as with the inorganics in solution and with water were estimated by Ming and Russell utilizing UNIQUAC functional group activity coefficients model (UNIFAC), where UNIQUAC stands for universal quasi chemical, which divides the organic components into

metagroups based on the functional group (oxygen, hydroxide, etc.) and the type of organic compound (monosaccharide, diacid, etc.). This allows nonlinear interactions to be estimated while minimizing the input parameters needed for the numerous possible organic constituents that can be found in atmospheric aerosols. Once the minimum Gibbs free energy is obtained, the growth factor of the aerosol, defined as the relative change in diameter of the wet aerosol compared to the dry aerosol, is calculated.

Initial modeling results by Ming and Russell compared well with laboratory results (Ming and Russell 2002). Nevertheless, it is not clear to what degree either the POEM code or similar quasi-parameterized approaches can be applied to the complex aerosols in the atmosphere. Our application of the model to our observations should be taken in the spirit of an exploratory, diagnostic study to better define the measurement and theoretical work necessary for complete success.

FLIP filters were chosen over TO filters for the POEM model closure studies in part due to the greater concentration of organics detected on the *FLIP* filter samples and in part due to the gravimetric mass closure results obtained for the *FLIP* filters. Because the air and the chemistry are considered comparable for the lowest level TO passes and *FLIP,* the output from the model calculation was compared to the γ values from the TO and therefore PCASP and FSSP aerosol size measurements from the TO.

The SCAPE2 aerosol model (Kim and Seinfeld 1995) was utilized for equilibrium calculations of the dry aerosol salt composition necessary for POEM initialization. The phosphate identified on the *FLIP* filters was not used in the model as the phosphate concentration levels could not be verified through either previous studies of marine aerosols nor through multidimensional laboratory techniques. Additionally, neither the SCAPE2 model nor the POEM model had the capacity for dealing with phosphate ions.

Due to the high sodium to sulfate ratio, even using the lowest assumed background concentration of ammonium of 30 ng m^{-3} (Quinn et al. 1996), the Simulating Composition of Atmospheric Particles at Equilibrium model, Version 2 (SCAPE2) model produced basic aerosols. This is likely reflective of the basic medium of the seawater (it is only through the dissolution of atmospheric gases such as sulfuric acid and formic acid into the wetted aerosol that the marine aerosol becomes acidic). As the *FLIP* aerosol samples were only roughly 15 m above MSL, the basic forms of the aerosols are plausible.

The basic dry aerosol components outputted by SCAPE2 contained sodium carbonate and sodium bicarbonate. However, neither the POEM code calculations of nonlinear energy interactions between ions nor the Pitzer and Clegg model upon which the code was based (Clegg et al. 1992) include estimates for carbonate interactions. In order to simulate both sodium and chloride mass closure, each filter output case was run twice for each data point, once with the sodium carbonate and sodium bicarbonate mass simply subsumed into the sodium chloride, and once with the sodium carbonate and sodium bicarbonate mass excluded from the model inputs. These runs produced an average difference of 0.06 in the resulting growth factors at identical relative humidities, with a maximum difference of 0.18.

In order to compare the model-outputted growth factor with the σ_{sp} measurements taken during RED, the size distributions measured by the PCASP and the FSSP during overpasses of *FLIP* by the TO were analyzed. The PCASP ran at 13°C higher temperature than ambient air, so the RH within the PCASP was determined from ambient air RH and temperature measurements.

The FSSP ran at ambient relative humidity. However, using the model-outputted growth factors to correct the size distributions to the diameters corresponding to the PCASP internal RH had the effect of propagating the model errors through the calculations twice: once while correcting the FSSP size distributions to the PCASP RH and once in the ensuing calculations to determine the γ parameter. In order to use in situ measurements of σ_{sp} to correct the FSSP-measured aerosol size distributions to diameters corresponding to the PCASP internal RH, the relationship between the growth factor and the γ scattering parameter was explored. The POEM calculated growth factor was used to calculate γ_D as defined in Eq. (3):

$$\frac{D_{\text{wet}}}{D_{\text{dry}}} = \left(\frac{1 - \text{RH}_{\text{wet}}/100}{1 - \text{RH}_{\text{dry}}/100}\right)^{-\gamma_D}, \tag{3}$$

where γ_D describes the relationship of the wet aerosol diameter, D_{wet}, and the dry aerosol diameter, D_{dry} at two RHs. Additionally, the Mie-calculated σ_{sp} associated with this growth factor, relative to ambient FSSP σ_{sp}, was determined and the corresponding γ was calculated. The linear dependence between γ_D and the scattering γ value was established using four observed filter compositional inputs with an R^2 value greater than 0.80 such that

$$\gamma = 7.515\ \gamma_D - 1.4689. \tag{4}$$

Once this relationship was determined γ_D was calculated from the γ associated with the *FLIP* filters derived from the UWPH nephelometer aboard the Twin Otter, and was used to correct the wet aerosol diameters measured by the FSSP to diameters corresponding to the humidity within the PCASP, which was 33% for both cases. The growth factor corrections to the observed aerosol size distributions were all relative to the growth factor at the PCASP internal RH.

The mean geometric diameter for each size bin was adjusted using the POEM output growth factor, and the scattering and extinction efficiency at 550 nm, Q_{scat} and Q_{ext}, were calculated from Mie theory (Wiscombe 1980). A refractive index of $1.55 + 1 \times 10^{-5}i$ was assumed for

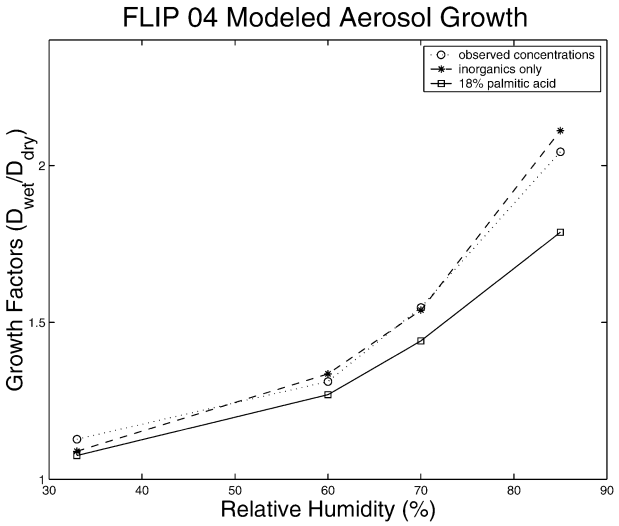

FIG. 11. Growth factor distributions for three different levels of organics. The first case (dotted line) shows the modeled growth factor using the chemical speciation observed on the FLIP 04 filter. The second case (dashed line) is the growth factor using the observed inorganics, but excluding any organics from the model input. The third case (solid line) is the growth factor resulting from chemical speciation input including 18% by mass palmitic acid.

the dry marine aerosols based on previous scattering studies (Quinn et al. 1996) and a volume-weighted average of the refractive index of the dry aerosol and of that of the water associated with the aerosol ($m = 1.33$) predicted by POEM was used in the Mie calculations. From this, scattering can be calculated with

$$\sigma_{sp} = \int_0^\infty Q_{scat}\, \pi r^2 N(r)\, dr, \qquad (5)$$

where $N(r)$ is the number density of particles of radius r. Once σ_{sp} at two different humidities are obtained, γ can easily be calculated using Eq. (1).

Two *FLIP* filters, FLIP 04 and FLIP 10, were chosen for extensive model runs. The chemically resolved mass contained 5% and 14% organics. FLIP 04 achieved 82% mass closure from gravimetric analysis and FLIP 10 achieved 90% mass closure, respectively. Initial runs at varied RHs were performed with the observed chemical concentrations (case 1), without any organics (case 2), and with synthetic mass closure using palmitic acid (case 3), a C16 carboxylic acid, to fill the observed discrepancy between chemically resolved and gravimetric mass. Palmitic acid was chosen as a proxy for mildly soluble carbon compounds because several recent studies have found it at significant concentrations in marine aerosols (Tervahattu et al. 2002; Kawamura et al. 2003).

A close examination of the growth factor output of the model for the FLIP 04 filter, illustrated in Fig. 11, shows that the three cases at four different relative humidities are reflective of the previously described effects of organics on hygroscopicity. The addition of the carboxylic acids and carbohydrates to the pure inorganic case increased aerosol growth at lower relative humidities by 3%, but equally inhibited growth at higher humidities, while palmitic acid suppressed the growth of the aerosol at all humidities.

The results of the Mie scattering calculations for the three different cases for the two *FLIP* filter studies are seen in Table 7. These can be compared to the observed σ_{sp} during corresponding TO overpasses, summarized in Table 8.

A few things must be noted when examining the data

TABLE 8. Observed Twin Otter σ_{sp} measurements and γ calculations corresponding to *FLIP* filter exposure times.

Instrument	σ_{sp} (Mm^{-1})	Std dev	RH
FLIP filter 04			
UWPH-1	35.4	0.47	86
UWPH-2	17.6	1.5	44
3-wavelength nephelometer	19.7	0.80	37
	Avg	Std dev	
γ	0.503	0.060	
FLIP filter 10			
UWPH-1	10.0	0.92	85
UWPH-2	6.41	0.66	43
3-wavelength nephelometer	7.43	0.85	36
	Avg	Std dev	
γ	0.326	0.057	

TABLE 7. Model-simulated scattering measurements, γ values, and associated errors ($\delta\gamma$) based upon *FLIP* filter-resolved chemical concentrations and PCASP and FSSP size distributions corresponding to *FLIP* filter exposure times. The γ values were calculated using the summed scattering of the fine and coarse mode. Case 1 is with the chemically resolved concentrations, case 2 contains no organics, and case 3 is run with palmitic acid to simulate mass closure.

	σ_{sp} (Mm^{-1})					
Case study	PCASP (RH = 33%)	PCASP (RH = 85%)	FSSP (RH = 33%)	FSSP (RH = 85%)	γ	$\delta\gamma$
FLIP 04, case 1	9.77	36.7	58.9	194	0.811	0.395
FLIP 04, case 2	9.77	42.5	59.4	213	0.874	0.251
FLIP 04, case 3	9.77	29.6	59.9	161	0.674	0.205
FLIP 10, case 1	3.14	13.4	27.7	89.1	0.803	0.170
FLIP 10, case 2	3.14	15.2	27.7	95.0	0.852	0.226
FLIP 10, case 3	3.14	12.1	28.1	83.9	0.750	0.383

presented in these tables. Although the relative humidities of the model do not correspond exactly to those of the measurements made in situ because the growth factor calculations were made relative to the PCASP internal RH, they are close enough that comparisons of the σ_{sp} can be made between the instruments and model. The modeled fine mode σ_{sp} captures less than half of the observed σ_{sp} for the dry scattering values. However, when the coarse mode σ_{sp} is added to the fine mode modeled σ_{sp} output, the result is significantly larger than the in situ measurements. This may be attributed to a number of factors, including the possibility that the FSSP is miscounting large aerosols. The FSSP was originally designed to count and bin cloud water droplets and the transformation to counting species with smaller diameters and different indices of refractions may not have been completely successful. This is supported by analysis of the mass closure studies performed on the filters. Whereas the aerosol volume concentration measured by the *FLIP* PCASP accounted for 95% and 69% of the gravimetric mass associated with FLIP 04 and FLIP 10 filters, respectively, the dry aerosol mass derived from the TO FSSP measurements associated with FLIP 04 was 3.7 times greater than the mass measured by the PCASP, and 6.9 times greater than the PCASP aerosol mass associated with FLIP 10. However, the overprediction of coarse mode σ_{sp} is uniform at both wet and dry humidities. Modeled values for f(RH), defined as the ratio of wet σ_{sp} (RH = 85%) to dry σ_{sp} (RH = 33%), range from 2.7 to 3.7. The measured f(RH) values corresponding to the two *FLIP* filters, where the relative humidity ratio is 86%–37% for FLIP 04 and 85%–36% for FLIP 10, range from 1.4 to 2.0. Because there is a significant coarse mode concentration and because the corresponding fractional change in σ_{sp} due to hygroscopic growth, although large, is not unreasonable, the σ_{sp} associated with the FSSP measurements was used in the γ calculations.

When comparing the three different model runs for each of the two case studies, the expected trends are observed. Without any organics, the wet σ_{sp} is enhanced and the observed γ value increases when compared to the run using the observed chemical concentrations. Although the modeled results are not able to mimic the observed σ_{sp}, the addition of palmitic acid improves the level of agreement significantly. The difference between the γ values obtained from the model and those obtained from the UWPH decreased from 59% to 57% for FLIP 10 and 38% to 25% for FLIP 04, whose model runs contained almost twice as much palmitic acid as FLIP 10. Nevertheless, agreement between the model and observations is poor.

Error analysis was performed on the modeled γ values through error propagation by Taylor series expansion of the γ equation. Errors intrinsic to the POEM model as summarized by Ming and Russell in Table 4 of their paper (Ming and Russell 2001) were estimated for the growth factor, as well as estimated errors due to the exclusion of sodium carbonate and sodium bicarbonate from the chemical speciation, which gave uncertainties in the growth factor of 0.01. Aerosol counting errors based upon the standard deviation of the FSSP and PCASP number distributions were included. These error calculations resulted in an uncertainty of the γ value of about 0.02 to 0.04. Measurements of the discrepancies of the FSSP sizing of aerosols during other field campaigns suggested the FSSP sizing error to be about 25% of the radius. When this error is propagated through the γ equation, errors as large as 0.39 are observed, as reported in Table 7.

4. Conclusions

Analysis of the data collected during the RED experiment has demonstrated the strong link between chemical composition of aerosols and their hygroscopic and light scattering behavior. The results of the multiple regression analysis using chemical predictors to approximate the sea salt and pollution contribution to the γ values and the 550-nm σ_{sp} demonstrate the low, but significant, contribution anthropogenic pollutants make to the hygroscopicity and scattering budgets of marine aerosols. Multiple regression analysis estimated that the anthropogenic aerosols in this venue are accountable for approximately 10% of the σ_{sp} for values correlated with the *FLIP* filters and 18% of the aerosol hygroscopicity and 21% of the σ_{sp} for values correlated with the TO filters. This is in contrast to GC models, which assume the air in the subtropical mid-Pacific to be essentially free of anthropogenic influence (Houghton et al. 2001, 392–393).

In an exploratory investigation of closure between measured aerosol hygroscopicity and hygroscopicity predicted from aerosol composition, case studies were performed on two filter samples taken aboard the *FLIP* and were correlated with σ_{sp} and size distribution measurements from overpasses of the *FLIP* research platform by the Center for Interdisciplinary Remotely Piloted Aircraft Studies (CIRPAS) TO aircraft. With chemical input that included all major inorganic constituents as well as four small-chained dicarboxylic acids and two carbohydrates, the POEM model reproduced the expected trends in the growth factors. When the growth factors were applied to the measured size distributions, the calculated σ_{sp}, even containing added palmitic acid to achieve mass closure, overpredicted the observed growth factor, most severely at higher RHs, producing γ values much higher than observed. This was likely primarily due to an overprediction of coarse mode σ_{sp} contributions due to sizing errors associated with the FSSP, as demonstrated in the error calculations. A more exact measurement of the coarse mode aerosol population is necessary to better reproduce observed scattering in model calculations. Other possible sources of error include the underprediction of the organic population within the chemical speciation of the aerosol

and the kinetic effects some organics may induce due to their surfactant nature. Changes to the ambient humidity of the air within the aircraft instrumentation after heating had occurred may not be reflected in the corresponding σ_{sp} due to this kinetic effect.

These results emphasize the important role slightly soluble organics play in aerosol hygroscopicity. Our results estimate that naturally occurring marine organics can account for 12% to 30% of aerosol mass, and other studies have suggested values ranging from 10% to 50%. More studies are needed to better quantify these organics, especially those with low water solubility, and to explore their role in aerosol growth and scattering properties.

Acknowledgments. Thanks to Dr. Lynn Russell and Dr. Yi Ming for sharing the POEM model code and answering all of the subsequent questions. Thanks to Dr. Athanasios Nenes for providing guidance with SCAPE2. We are also grateful to Dr. Kenn Anderson (SPAWAR Systems Center, San Diego) for his organization of the RED campaign. Support for this research was provided by ONR Grant N00014-97-1-0132 and NSF Grant ATM 9908471.

REFERENCES

Adams, P. J., and J. H. Seinfeld, 1999: Global concentrations of tropospheric sulfate, nitrate and ammonium aerosol simulated in a general circulation model. *J. Geophys. Res.,* **104,** 13 791–13 823.

Albrecht, B. A., M. P. Jensen, and W. J. Syrett, 1995: Marine boundary layer structure and fractional cloudiness. *J. Geophys. Res.,* **100,** 14 209–14 222.

Aluwihare, L. I., D. J. Repeta, and R. F. Chen, 1997: A major biopolymeric component to dissolved organic carbon in surface sea water. *Nature,* **387,** 166–169.

Anderson, T. A., and J. A. Ogren, 1998: Determining aerosol radiative properties using the TSI 3563 integrating nephelometer. *Aerosol Sci. Technol.,* **29,** 57–69.

Bigg, E. K., 1986: Discrepancy between observation and prediction of concentrations of cloud condensation nuclei. *Atmos. Res.,* **20,** 80–86.

Charlson, R. J., S. E. Schwartz, J. M. Hales, R. D. Cess, J. A. Coakley Jr., J. E. Hansen, and D. J. Hoffmann, 1992: Climate forcing by anthropogenic aerosols. *Science,* **255,** 423–430.

Clarke, A. D., and V. N. Kapustin, 2003: The Shoreline Environment Aerosol Study (SEAS): A context for marine aerosol measurements influenced by a coastal environment and long-range transport. *J. Atmos. Oceanic Technol.,* **20,** 1351–1361.

Clegg, S. L., K. S. Pitzer, and P. Brimblecombe, 1992: Thermodynamics of multicomponent, miscible, ionic solutions. 2. Mixtures including unsymmetrical electrolytes. *J. Phys. Chem.,* **96,** 9470–9479.

Draxler, R. R., cited 1997: HYbrid single-particle Langragian integrated trajectory model. [Available online at http://www.arl.noaa.gov/ready/hysp_info.html.]

Ellison, G. B., A. F. Tuck, and V. Vaida, 1999: Atmospheric processing of organic aerosols. *J. Geophys. Res.,* **104,** 11 633–11 641.

Fraser, M. P., and K. Lakshmanan, 2000: Using levoglucosan as a molecular marker for the long-range transport of biomass combustion aerosols. *Environ. Sci. Technol.,* **34,** 4560–4564.

Gao, S., and Coauthors, 2001: Experimental and modeling studies of secondary organic aerosol formation and some applications to the marine boundary layer. *J. Geophys. Res.,* **106,** 27 619–27 634.

——, D. A. Hegg, and H. Jonsson, 2003: Aerosol chemistry, and light-scattering and hygroscopicity budgets during outflow from East Asia. *J. Atmos. Chem.,* **46,** 55–88.

Gassó, S., and Coauthors, 2000: Influence of humidity on the aerosol scattering coefficient and its effect on the upwelling radiance during ACE-2. *Tellus,* **52B,** 546–567.

Houghton, J. T., Y. Ding, D. J. Griggs, M. Noguer, P. J. van der Linden, X. Dai, K. Maskell, and C. A. Johnson, Eds., 2001: *Climate Change 2001: The Scientific Basis.* Cambridge University Press, 881 pp.

Katzen, F., 1969: Visibility forecast in the phase of pre-condensation. *Tellus,* **21,** 631–635.

Kawamura, K., and F. Sakaguchi, 1999: Molecular distribution of water soluble dicarboxylic acids in marine aerosols over the Pacific Ocean including the Tropics. *J. Geophys. Res.,* **104,** 3501–3509.

——, Y. Ishimura, and K. Yamazaki, 2003: Four years' observations of terrestrial lipid class compounds in marine aerosols from the western North Pacific. *Global Biogeochem. Cycles,* **17,** 1003, doi:10.1029/2001GB001810.

Kim, Y. P., and J. H. Seinfeld, 1995: Atmospheric gas–aerosol equilibrium. III: Thermodynamics of crustal elements Ca^{2+}, K^{+}, and Mg^{2+}. *Aerosol Sci. Technol.,* **22,** 93–110.

Liu, P., W. Leaitch, J. Strapp, and M. Wasey, 1992: Response of particle measuring systems airborne ASASP and PCASP to NaCl and latex particles. *Aerosol Sci. Technol.,* **16,** 83–95.

Maßling, A., A. Weidensohler, B. Busch, C. Neusüß, P. Quinn, T. Bates, and D. Covert, 2003: Hygroscopic properties of different aerosol types over the Atlantic and Indian Ocean. *Atmos. Chem. Phys.,* **3,** 1377–1397.

McGovern, F. M., F. Raes, R. Van Dingenen, and H. Maring, 1999: Anthropogenic influences on the chemical and physical properties of aerosols in the Atlantic subtropical region during July 1994 and July 1995. *J. Geophys. Res.,* **104,** 14 309–14 319.

McInnes, L. M., D. S. Covert, P. K. Quinn, and M. S. Germani, 1994: Measurements of chloride depletion and sulfur enrichment in individual sea-salt particles collected from the remote marine boundary layer. *J. Geophys. Res.,* **99,** 8257–8268.

Ming, Y., and L. M. Russell, 2001: Predicted hygroscopic growth of sea salt aerosols. *J. Geophys. Res.,* **106,** 28 259–28 274.

——, and ——, 2002: Thermodynamic equilibrium of organic-electrolyte mixtures in aerosol particles. *AICE J.,* **48,** 1331–1348.

Oppo, C. S., S. Bellandi, N. D. Innocenti, A. M. Stortini, G. Loglio, E. Schiavuta, and R. Cici, 1999: Surfactant components of marine organic matter as agents for biogeochemical fractionation and pollution transport via marine aerosols. *Mar. Chem.,* **63,** 235–253.

Penner, J., C. C. Chuang, and K. Grant, 1998: Climate forcing by carbonaceous and sulfate aerosols. *Climate Dyn.,* **14,** 839–851.

Quinn, P. K., D. S. Covert, T. S. Baster, V. N. Kapustin, D. C. Ramsey-Bell, and L. M. McInnes, 1993: Dimethylsulfide/cloud condensation nuclei/climate system: Relevant size-resolved measurements of the chemical and physical properties of atmospheric aerosol particles. *J. Geophys. Res.,* **98,** 10 411–10 427.

——, V. N. Kapustin, and T. S. Bates, 1996: Chemical and optical properties of marine boundary layer aerosol particles of the mid-Pacific in relation to sources and meteorological transport. *J. Geophys. Res.,* **101D,** 6931–6951.

Reid, J. S., H. Jonsson, M. Smith, and A. Smirnov, 2001: Evolution of the vertical profile and flux of large sea-salt particles in a coastal zone. *J. Geophys. Res.,* **106,** 12 039–12 053.

——, and Coauthors, 2003: Comparison of size and morphological measurements of coarse mode dust particles from Africa. *J. Geophys. Res.,* **108,** 8593, doi:10.1029/2002JD002485.

Simoneit, B. R. T., J. J. Schauer, C. G. Nolte, D. R. Oros, V. O. Elias, M. P. Frasier, W. F. Rogge, and G. R. Cass, 1999: Levoglucosan, a tracer for cellulose in biomass burning and atmospheric particles. *Atmos. Environ.,* **33,** 173–182.

Ten Harkel, M., 1997: The effects of particle-size distributions and chloride depletion of sea-salt aerosols on estimating atmospheric deposition at a coastal site. *Atmos. Environ.*, **31,** 417–427.

Tervahattu, H., J. Juhanoja, and K. Kupianinen, 2002: Identification of an organic coating on marine aerosol particles by TOF-SIMS. *J. Geophys. Res.*, **107D,** 4319, doi:10.1029/2001JD001403.

Wiscombe, W. J., 1980: Improved Mie scattering algorithms. *Appl. Opt.*, **19,** 1505–1509.

Xiong, J. Q., M. H. Zhong, C. P. Fang, L. C. Chen, and M. Lippman, 1998: Influence of organic films on the hygroscopicity of ultrafine sulfuric acid aerosol. *Environ. Sci. Technol.*, **32,** 3536–3541.